Mechanics and Chemistry: Single Molecule Bond Rupture Forces Correlate with Molecular Backbone Structure

Michael Frei,[†] Sriharsha V. Aradhya,[†] Max Koentopp,[‡,||] Mark S. Hybertsen,[*,§] and L. Venkataraman[*,†,‡]

[†]Department of Applied Physics and Applied Mathematics, [‡]Center for Electron Transport in Molecular Nanostructures, Columbia University, New York, New York, United States

[§]Center for Functional Nanomaterials, Brookhaven National Laboratories, Upton, New York, United States

S *Supporting Information*

ABSTRACT: We simultaneously measure conductance and force across nanoscale junctions. A new, two-dimensional histogram technique is introduced to statistically extract bond rupture forces from a large data set of individual junction elongation traces. For the case of Au point contacts, we find a rupture force of 1.4 ± 0.2 nN, which is in good agreement with previous measurements. We then study systematic trends for single gold metal—molecule—metal junctions for a series of molecules terminated with amine and pyridine linkers. For all molecules studied, single molecule junctions rupture at the Au—N bond. Selective binding of the linker group allows us to correlate the N—Au bond-rupture force to the molecular backbone. We find that the rupture force ranges from 0.8 nN for 4,4′ bipyridine to 0.5 nN in 1,4 diaminobenzene. These experimental results are in excellent quantitative agreement with density functional theory based adiabatic molecular junction elongation and rupture calculations.

KEYWORDS: Molecular conductance, force spectroscopy, gold point-contact, bond rupture, break-junction
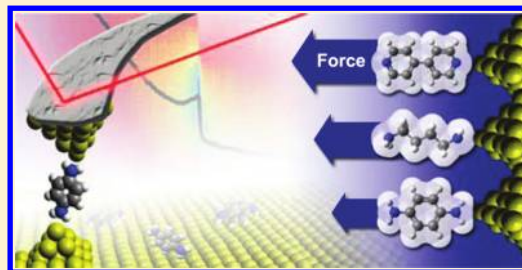
Understanding physical properties of single molecule junctions is of fundamental importance to nanoscale electronics.[1] While electrical and thermal properties have been probed in a variety of organic molecules bound to metal electrodes,[2−8] measurements of rupture forces of single metal-molecule-metal junctions are new,[9,10] and simple predictions relating the mechanics of these junctions to the backbone chemistry have not been tested. Here, we use a modified atomic force microscope (AFM) to form single molecule junctions between a gold substrate and a gold-coated cantilever. The simultaneously measured conductance and force between the AFM tip and substrate are analyzed to determine bond rupture forces. We use a new technique to analyze force data to obtain bond rupture forces from a large, statistically significant set of individual junction elongation traces. Using this method, we first show that the force required to break a gold—gold bond is 1.4 nN, based on over 38 000 measurements and in good agreement with previous published results.[11] We then show that for single molecule junctions, the N—Au bond-rupture force depends on the molecular backbone, and varies from 0.8 nN for 4,4′ bipyridine to 0.5 nN in 1,4 diaminobenzene. There results are supported by density functional theory calculations for adiabatic junction elongation trajectories. Bond rupture forces determined from these calculations agree quantitatively with the experimental results.

We simultaneously measure the conductance and force of molecular junctions by repeatedly forming Au point contacts with a modified home-built conductive atomic force microscope (AFM) described in detail in the Supporting Information. All molecules were obtained from Sigma-Aldrich and were used without further purification. Conductance is determined by measuring current through the junction at a constant applied bias of 25 mV for short molecules and 75 mV for 1,6-hexanediamine and for 4,4′ bipyridine. Simultaneous measurements of cantilever deflection relate to the force applied across the junction (Figure 1A). The AFM is operated in ambient conditions at room temperature.

For each measurement, a gold point-contact is first formed between the substrate and cantilever. It is then pulled apart and broken in an environment of molecules while conductance and force are measured as a function of sample displacement. This process is repeated thousands of times to obtain large data sets of conductance and simultaneously acquired force traces. Before adding a molecule to the substrate, at least 1000 conductance traces were collected to ensure that no contamination was present in the setup. Individual conductance traces for a gold point-contact show stepwise decrease in conductance until a single atom contact is formed with a conductance of $G_0 = 2e^2/h$, the quantum of conductance (Figure 1B). The simultaneously acquired force traces show a characteristic sawtooth pattern (Figure 1B) indicating two distinct force regimes: gradual linear increases due to elastic (reversible) elongations and sharp drops due to permanent deformations of the junction. Upon further
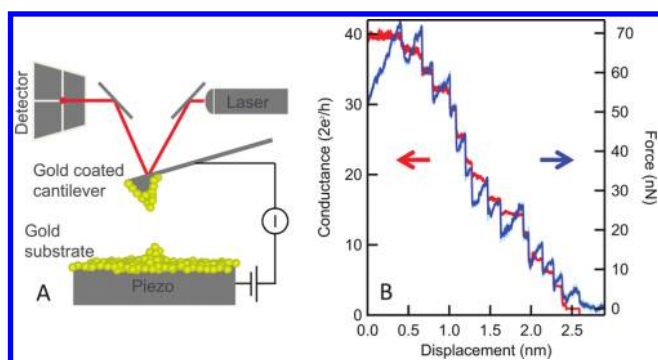
Figure 1. (A) Schematic of the modified conductive atomic force microscope. A gold−gold junction is formed between a Cr/Au-coated cantilever and an Au-coated substrate with the relative separation controlled by a piezo. The force acting on the junction is detected by optically measuring the deflection of the cantilever. (B) Sample conductance (red) and force (blue) data of a breaking gold junction collected at a bias of 25 mV and a piezo displacement speed of 18 nm/s. The light blue force trace is raw data, while the dark blue trace has been smoothed. Step-wise decreases in conductance are accompanied by sudden jumps in the force.

Figure 2. (A) Two-dimensional conductance histogram constructed from over 38 000 traces. All traces are aligned such that the end of the plateau at G_0 is at zero along the displacement axis. A large number of counts is visible at integer multiples of G_0. Inset: Sample conductance trace aligned to zero displacement at the end of the G_0 plateau. (B) Two-dimensional force histogram constructed from simultaneously acquired force traces. The force profile (red curve) is overlaid and shows a clear jump at zero displacement. The rupture force of 1.4 nN for a single atomic contact is determined by extrapolating the fit of the force profile (dotted line). Inset: Force trace acquired simultaneously with conductance trace shown in the inset to panel A, aligned after the G_0 break. The light blue trace is the raw signal and the dark blue is smoothed force data.

stretching, the single atomic gold wire breaks and the conductance exhibits a tunneling signature when no molecules are present, while the cantilever displacement changes abruptly. When measurements are carried out in an environment of molecules, an additional conductance step is frequently observed at a molecule dependent conductance value below $1G_0$ along with an additional abrupt change in the force trace. The full trace of force versus elongation presents a rich data set describing the mechanical evolution of these junctions under stress. In this study, we focus on the force associated with the breaking of a single atomic gold contact or a gold−molecule−gold junction. This can be determined by analyzing the cantilever deflection at the location where the $1G_0$ or the molecular conductance step ends and the junction breaks.

To extract statistically significant characteristics from the evolution of junction conductance and force as a function of sample displacement, we construct two-dimensional (2D) histograms from the conductance and force traces, setting the origin of the displacement axis at the point where either the $1G_0$ conductance step or the molecular conductance step breaks. This well-defined position on the x-axis was determined individually for each trace, using an unbiased automated algorithm (see Supporting Information). A fraction of the traces do not show a conductance plateau at G_0 or a plateau corresponding to a molecular junction. It is likely that the absence of the G_0 or the molecular conductance plateau means that a single-atom point contact or a single molecule junction was not formed during that trace. Therefore, these traces were not used for further analysis as they do not contain the bond rupture event of interest (see Supporting Information Figure 1 for sample rejected traces). The statistical occurrence of the targeted junction varies with the case and will be noted below, but a statistically significant and unbiased data set results in each case. Each data point on the digitized conductance (force) trace was thus assigned a conductance (force) coordinate (along the y-axis) and a position coordinate (along the x-axis). Two-dimensional conductance histograms were then generated without further analysis. For the two-dimensional force histogram, we also set the force at the new zero-displacement position to zero force by subtracting an offset
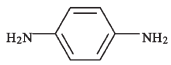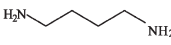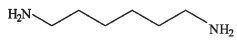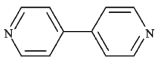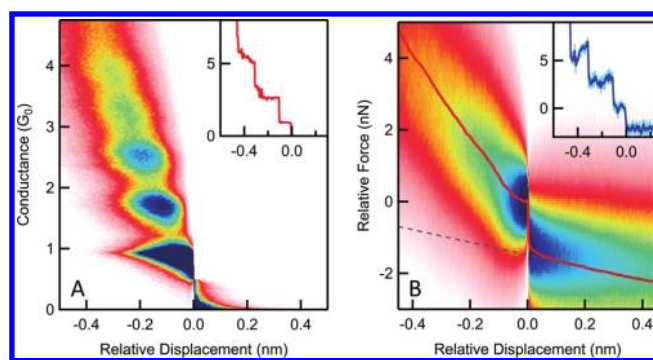
from the entire force trace. This realigned all force traces to a common point such that each force and displacement value was now determined relative to that at the end of the conductance step in each trace. After this realignment, thousands of force traces were added to generate a two-dimensional force histogram. A statistically averaged force profile is obtained from this histogram from the peak of a Gaussian that is fit to vertical sections at every displacement bin.

Figure 2A,B shows two-dimensional conductance and force histograms, respectively, constructed from over 38 000 traces measured without any molecules present and using approximately 20 different tip/sample pairs. Insets to Figure 2A,B show a sample conductance and simultaneously acquired force trace, respectively, to illustrate where zero in displacement is set. The conductance or force (y-) axis and the position axis (x-) use linear bins in these plots. Negative displacements are events that occur before the end of the $1G_0$ plateau while positive corresponds to data acquired after the end of the plateau. These histograms are generated from traces where the G_0 step can be identified with our automated algorithm (see Supporting Information). Approximately 75% (38 000 out of 49 500) of the measured traces exhibit a clearly identifiable G_0 step and are included. Figure 2A shows clear peaks at integer multiples of G_0 occurring at negative displacements, and almost no counts at positive displacements, since zero displacement is set at the point when the G_0 contact breaks.

The 2D force histogram, created from the same set of traces, (Figure 2B) shows a trend in the force that is decreasing with increasing displacement with a clear sharp drop at zero displacement. The force required to break the G_0 contact can be determined from the magnitude of this drop. The force profile is effectively an averaged force trace for the single atom contact rupture event. It shows a clearly defined drop of 1.4 ± 0.2 nN at zero displacement, as illustrated in Figure 2B, corresponding to the breaking force of a single Au−Au bond. This value is in good agreement with published results,[11,12] demonstrating that our 2D analysis method agrees with the conventional method of

Table 1

Molecule	Structure	Conductance (G_0)	Bond Rupture Force (nN)	
			Experiment	Theory
1,4 Benzene-diamine	H_2N—⬡—NH_2	6.2×10^{-3}	0.53 ± 0.09	0.46
1,4 Butane-diamine	H_2N ⌇ NH_2	9.0×10^{-4}	0.69 ± 0.06	0.84
1,6 Hexane-diamine	H_2N ⌇ NH_2	1.1×10^{-4}	0.62 ± 0.09	N/A
4,4' Bipyridine	N—⬡—⬡—N	1.0×10^{-4}	0.80 ± 0.08	1.00

determining a force drop on a trace by trace basis (see Supporting Information). However, we note here that the present analysis method is not biased toward larger force drops which are easier to identify if individual traces are analyzed. Furthermore, this breaking force is determined from a statistically significant data set of about 38 000 traces, providing the first robust and unbiased determination of the single Au—Au bond breaking force.

We now use this same technique to measure bond rupture force in single molecule junctions with four different molecules as listed in Table 1. Three are amine (NH_2) terminated molecules, 1,4-benzenediamine, 1,4-butanediamine, and 1,6-hexanediamine, which bind selectively to undercoordinated gold through a donor−acceptor bond between the terminal N and Au atom.[13] The fourth is 4,4′-bipyridine, which also binds through an N−Au donor−acceptor bond.[14] Molecules are evaporated onto the Au-on-mica substrates, and for each molecule over 30 000 conductance and simultaneously acquired force traces are collected with multiple tip/sample pairs. Conductance and force measurements are analyzed by generating 2D histograms as detailed above for the molecular breaking force.

Figure 3A shows a 2D conductance histogram for 1,4-butanediamine where the origin in the displacement axis is set at the end of the molecular conductance step. Logarithmic bins for the conductance (y-) axis and linear bins for the displacement (x-) axis are chosen for image clarity. The measured traces that show a molecular conductance step were selected using an automated algorithm (see Supporting Information) for both conductance and force analysis. Insets of Figure 3A,B show conductance and simultaneous force data for one particular junction breaking event. Approximately 30% of the 31 000 measured traces showed evidence of full single molecule junction formation and contribute to the histogram. A clear peak is seen in the conductance histogram at 9×10^{-4} G_0, which gives us the most probable conductance of a gold−1,4-butanediamine−gold junction. This peak extends over a displacement of about 0.15 nm, indicating that molecular junctions can be elongate over this distance prior to the final rupture. Conductance histograms for measurements with all other molecules are shown in the Supporting Information (Figures S3A−S5A). Of the four molecules measured, the three diamines show a single conductance peak due to the selective binding of the NH_2 linker to undercoordinated gold atoms.[13,15]
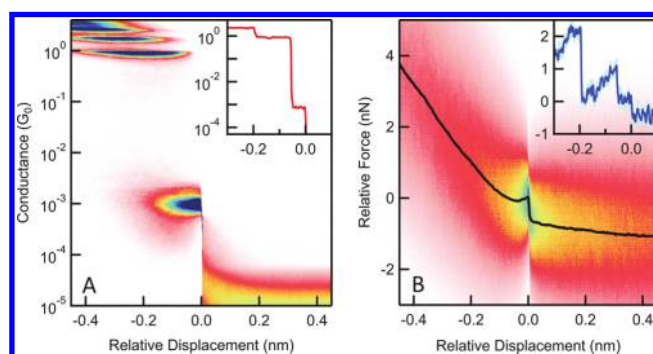

Figure 3. (A) Two-dimensional conductance histogram of 1,4-butanediamine data constructed from over 10 000 traces with a molecular conductance step. The conductance data is presented on a log scale. Features representing a sequence of gold contacts clearly appear at integer multiples of G_0. A molecular signature can be clearly seen at 1×10^{-3} G_0. Inset: A sample conductance trace showing a G_0 and molecular plateau with zero displacement set to the end of the molecular plateau. (B) The two-dimensional force histogram for 1,4-diaminobutane is constructed from the set of simultaneously acquired force traces used to construct the conductance histogram. The average force profile (black curve) shows a clear drop at zero-displacement, which gives a statistically determined breaking force for the N−Au bond of 0.69 nN. Inset: The simultaneously acquired force trace aligned after the molecular step is shown both unsmoothed (light blue) and smoothed (dark blue). Force events corresponding to a G_0 rupture and molecular breaking are clearly visible.

4,4′-Bipyridine shows two conductance peaks (a high-G and a low-G peak) that occur at distinct junction elongation distances. In this work, we probe the rupture from the low-G peak, which corresponds to a geometry where the molecule bridges the two gold electrodes vertically.[14] All conductance peak positions for these four molecules are close to previously published data (see Table 1) collected in solution using the scanning tunneling microscope-based break junction technique.[14,15] This validates our measurement setup and the molecule deposition technique. Furthermore, the clear conductance signature seen for all these molecules allows us to measure these specific single gold-molecule-gold junction rupture events unambiguously.
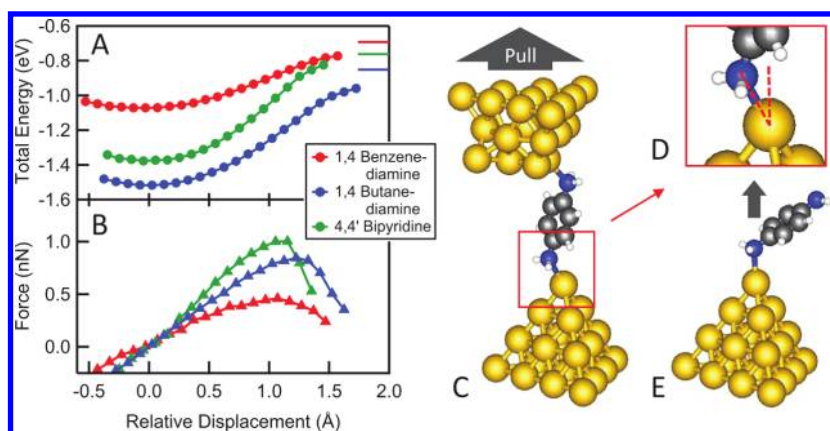
Figure 4. (A) Calculated total energy curves from adiabatic trajectories for 1,4-benzenediamine (red), 1,4-butanediamine (blue), and 4,4′-bipyridine (green) shown as a function of displacement. Bars shown at right indicate the asymptotic values. (B) Calculated applied force curves for the same molecules shown against displacement display the same trend as the experimental results. (C) Junction structure showing a 1,4-benzenediamine junction at 0.1 nm elongation relative to the local energy minimum. (D) Zoom in of the Au−N bond indicating bond angle with respect to pulling direction. (E) Sample structure used to investigate a single Au−N bond force profile for 1,4-benzenediamine bound to a gold electrode with bond aligned to the pulling direction.

Figure 3B shows the corresponding 2D force histogram created from the force traces acquired simultaneously with the conductance traces used to create the histogram in Figure 3A. Force histograms for all other molecules are shown in Supporting Information (Figures S3B−S5B). Since the origin in the displacement axis is set at the point where the molecular conductance step ends, the drop in the force profile, shown overlaid on the 2D histogram, corresponds to the average force required to rupture the gold−molecule−gold junction. This force is determined to be 0.69 nN ± 0.06 nN for 1,4-butanediamine, where the error bar represents the standard deviation of the measured force from five different tip/sample pairs. This force is significantly smaller than the force required to break the gold−gold bond. Although the conductance steps extended over 0.15 nm as seen in Figure 3A, we see no signature in the force histogram over this range that would indicate statistically reproducible force events at a well-defined displacement prior to junction rupture. However, individual traces do show additional force features indicating that during the junction elongation process, bond breakage or other atomic rearrangements do occur.[16] These force measurements thus provide new insight into the junction evolution confirming experimentally that the molecular junction ruptures at the Au−N bond.

In Table 1, we show bond rupture forces determined from 2D force histograms for all four molecules considered here. We see that in all cases, the gold−molecule−gold junction ruptures at a force smaller than that of a gold−gold bond, indicating that rupture occurs at the Au−N donor−acceptor bonds consistent with earlier work.[10] Comparing the measured rupture forces we see first that for the two alkanes with 4 and 6 carbons in the backbone, the rupture forces are very similar. Additionally, we see that the force required to break the N−Au bond in the conjugated molecule, 1,4-benzenediamine, is considerably smaller than in 1,4-butanediamine and 1,6-hexanediamine, which are fully saturated.

To better understand these results, we have carried out density functional theory (DFT) based calculations simulating the junction elongation and rupture process[17,18] for three of the four molecules studied here, excluding the longer alkane. The Au tip and surface were modeled with Au pyramids (20 atoms each) with (111) surfaces. The tip atom on the top pyramid was moved

to an adatom site on one facet resulting in a blunt, three atom tip. These model structures were previously used to analyze extended elongation trajectories.[16] Here we focused on the portion of the trajectory where the junction was elongated from a local energy minimum through the inflection point and finally probed the dissociated structure after one bond ruptures. The back layer of Au atoms in each pyramid was held fixed with a bulk lattice parameter 4.08 Å. All other degrees of freedom were relaxed until all forces were less than 0.005−0.01 eV/Å for each junction structure. The junction was elongated in steps of 0.1 Å by increasing the separation between the pyramids along the z direction and then fully optimizing the geometry. As the point of maximum force was approached for the 4,4′-bipyridine junction, competing structures were examined to identify that with the lowest energy, while in the other junctions the lowest energy structure emerged naturally at each step. Density functional theory total energy calculations and geometry optimization were performed with the VASP package,[19] using the projector augmented wave approach which naturally included scalar relativistic effects for gold[20,21] and the generalized gradient approximation (GGA) of Perdew, Burke, and Ernzerhof (PBE)[22] for the exchange-correlation density functional. The model junction was placed in a hexagonal supercell ($a = 2.0$ nm, $c = 3.5$ nm) and the basis set for solution of the Kohn−Sham equations was determined by a 400 eV cutoff. The accuracy of the GGA for calculation of donor−acceptor binding energy, such as the amine−Au bond here, has been tested in specific examples. Comparison to carefully converged coupled-cluster calculations for the Au−NH_3 molecular complex showed that GGA calculations underestimate the binding energy by about 0.11−0.13 eV.[23] Analyses of ammonia and pyridine adsorption on the Au(111) surface are also consistent with at least an 0.1 eV underestimate.[24,25] The present calculations with a well-converged basis set gave a Au−N bond energy that was about 0.2 eV smaller than that obtained previously with the def2-SVP basis in TurboMole,[16] the latter being a less complete basis and exhibiting some basis set superposition error in the binding energy.

Total energy and applied force computed from adiabatic junction elongation trajectories for each molecule are shown in Figure 4A,B. All three junctions were studied using the same Au

structure and link attachment points to highlight the chemical trends, as illustrated in Figure 4C. We see that in all cases, the junction ruptures at the Au—N bond, as observed in the experiment. The maximum calculated sustained force determined for each molecule is reported in Table 1. We see that 1,4-benzenediamine can sustain the smallest force, while 4,4′-bipyridine can sustain the largest, which is in good quantitative agreement with the measured trends, and for 4,4′-bipyridine this is in good agreement with earlier DFT-based studies.[26]

These calculated forces are the largest sustainable breaking forces calculated from a single adiabatic junction elongation trajectory. However, previous studies[16] showed that small changes in junction structure (attachment point or molecule orientation) can lead to ~0.1−0.2 nN variations in the maximum sustained force. More generally, we expect that diverse junction structures are sampled in the experiments, including variations in Au—N bond orientation in the junction and relative to the pulling direction (Figure 4D).

To probe the importance of the bond orientation on the maximum sustained force, we also studied the elongation of a single N—Au bond for a well-aligned model structure, as illustrated for the 1,4-benzenediamine case in Figure 4E. Stretching the N—Au bond by constraining the position of the bound N and the back plane of the Au pyramid structure resulted in a calculated maximum sustained force of 0.83, 1.09, and 1.12 nN for 1,4-benzenediamine, 1,4-butanediamine and 4.4′-bipyridine, respectively (see Supporting Information Figure S6 for full trajectories). Thus, the force required to rupture the Au—N bond depends on the backbone chemistry. In 1,4-benzenediamine, the N lone-pair is partly delocalized into the π-system, which weakens the N—Au donor−acceptor bond. In saturated molecules, or in pyridines, where the lone-pair is orthogonal to the π-system, the lone-pair is fully available for binding, resulting in larger rupture forces. However, the differences between 1,4-butanediamine and 4,4′-bipyridine are more subtle. While an sp^3 derived lone pair of 1,4-butanediamine is more sharply directed in space than an sp^2 derived lone pair in 4,4′-bipyridine, the availability of the π-space on the pyridine contributes to the binding.[27,28] As a consequence, the binding energies and maximum sustained forces are similar.

Comparing the single Au—N bond rupture forces listed above with those for the junctions listed in Table 1, we see that the impact of Au—N bond orientation (Figure 4D) is most prominent for 1,4-benzenediamine and least important for 4,4′-bipyridine. In 4,4′-bipyridine, the N lone-pair orbital is oriented in the plane of the rings allowing for a vertical molecule geometry,[29] thus the calculations for the junction and the bond are very close. For 1,4-butanediamine and 1,4-benzenediamine junctions, which naturally result in geometries where the backbone and the N—Au bond are tilted, the component of the force projected on the junction elongation direction (vertical) will be reduced by the direction cosine. This will be more significant for 1,4-benzenediamine and 1,4-butanediamine than for 4,4′-bipyridine. Indeed, we find that although Au—N bond rupture forces for 4,4′-bipyridine and 1,4-butanediamine are very similar, the experiment and trajectory based calculated show that 1,4 butanediamine junctions rupture at smaller forces.

In summary, we demonstrated an experimental approach to simultaneously measuring force and conductance data for single molecular junctions, developing and establishing a new, 2D histogram method to statistically evaluate thousands of force measurements. This method leads to an experimentally determined average breaking force of a single Au—Au bond of 1.4 nN, based on over 38 000 individual measurements. We measure the average breaking force for amine and pyridine terminated molecules. Finally, we show that the electronic structure of the molecular backbone alters N—Au bond strengths considerably, as can be seen both in the calculations and in the measurements: 1,4-benzenediamine binds most weakly to Au atoms, while the pyridine−gold bond exhibits the largest breaking force among the molecules considered here.

■ ASSOCIATED CONTENT

Ⓢ Supporting Information. Experimental details, additional figures, and additional references. This material is available free of charge via the Internet at http://pubs.acs.org.

■ AUTHOR INFORMATION

Corresponding Author
*E-mail: (M.S.H.) mhyberts@bnl.gov; (L.V.) lv2117@columbia.edu.

Present Addresses
‖Q-Cells SE, OT Thalheim, Sonnenallee 17 - 21, 06766 Bitterfeld-Wolfen, Germany.

■ ACKNOWLEDGMENT

■ REFERENCES

(1) Joachim, C.; Ratner, M. A. *Proc. Natl. Acad. Sci. U.S.A.* **2005**, *102* (25), 8801−8808.

(2) Reed, M. A.; Zhou, C.; Muller, C. J.; Burgin, T. P.; Tour, J. M. *Science* **1997**, *278* (5336), 252−254.

(3) Smit, R. H. M.; Noat, Y.; Untiedt, C.; Lang, N. D.; van Hemert, M. C.; van Ruitenbeek, J. M. *Nature* **2002**, *419* (6910), 906−909.

(4) Reichert, J.; Ochs, R.; Beckmann, D.; Weber, H. B.; Mayor, M.; von Lohneysen, H. *Phys. Rev. Lett.* **2002**, *88* (17), No. 176804.

(5) Xu, B. Q.; Tao, N. J. J. *Science* **2003**, *301* (5637), 1221−1223.

(6) Venkataraman, L.; Klare, J. E.; Nuckolls, C.; Hybertsen, M. S.; Steigerwald, M. L. *Nature* **2006**, *442* (7105), 904−907.

(7) Baheti, K.; Malen, J. A.; Doak, P.; Reddy, P.; Jang, S. Y.; Tilley, T. D.; Majumdar, A.; Segalman, R. A. *Nano Lett.* **2008**, *8* (2), 715−719.

(8) Reddy, P.; Jang, S. Y.; Segalman, R. A.; Majumdar, A. *Science* **2007**, *315* (5818), 1568−1571.

(9) Grandbois, M.; Beyer, M.; Rief, M.; Clausen-Schaumann, H.; Gaub, H. E. *Science* **1999**, *283* (5408), 1727−1730.

(10) Xu, B. Q.; Xiao, X. Y.; Tao, N. J. *J. Am. Chem. Soc.* **2003**, *125* (52), 16164−16165.

(11) Rubio, G.; Agrait, N.; Vieira, S. *Phys. Rev. Lett.* **1996**, *76* (13), 2302−2305.

(12) Tavazza, F.; Levine, L. E.; Chaka, A. M. *J. Appl. Phys.* **2009**, *106* (4), No. 043522.

(13) Venkataraman, L.; Klare, J. E.; Tam, I. W.; Nuckolls, C.; Hybertsen, M. S.; Steigerwald, M. L. *Nano Lett.* **2006**, *6* (3), 458−462.

(14) Quek, S. Y.; Kamenetska, M.; Steigerwald, M. L.; Choi, H. J.; Louie, S. G.; Hybertsen, M. S.; Neaton, J. B.; Venkataraman, L. *Nat. Nanotechnol.* **2009**, *4* (4), 230–234.

(15) Park, Y. S.; Whalley, A. C.; Kamenetska, M.; Steigerwald, M. L.; Hybertsen, M. S.; Nuckolls, C.; Venkataraman, L. *J. Am. Chem. Soc.* **2007**, *129* (51), 15768–15769.

(16) Kamenetska, M.; Koentopp, M.; Whalley, A.; Park, Y. S.; Steigerwald, M.; Nuckolls, C.; Hybertsen, M.; Venkataraman, L. *Phys. Rev. Lett.* **2009**, *102* (12), No. 126803.

(17) Paulsson, M.; Krag, C.; Frederiksen, T.; Brandbyge, M. *Nano Lett.* **2009**, *9* (1), 117–121.

(18) Qi, Y. H.; Qin, J. Y.; Zhang, G. L.; Zhang, T. *J. Am. Chem. Soc.* **2009**, *131* (45), 16418–16422.

(19) Kresse, G.; Furthmuller, J. *Phys. Rev. B* **1996**, *54* (16), 11169.

(20) Kresse, G.; Joubert, D. *Phys. Rev. B* **1999**, *59* (3), 1758–1775.

(21) Blochl, P. E. *Phys. Rev. B* **1994**, *50* (24), 17953–17979.

(22) Perdew, J. P.; Burke, K.; Ernzerhof, M. *Phys. Rev. Lett.* **1996**, *77* (18), 3865–3868.

(23) Lambropoulos, N. A.; Reimers, J. R.; Hush, N. S. *J. Chem. Phys.* **2002**, *116* (23), 10277–10286.

(24) Bilic, A.; Reimers, J. R.; Hush, N. S. *J. Chem. Phys.* **2005**, *122* (9), 094708.

(25) Bilic, A.; Reimers, J. R.; Hush, N. S. *J. Phys. Chem. B* **2002**, *106* (26), 6740–6747.

(26) Stadler, R.; Thygesen, K. S.; Jacobsen, K. W. *Phys. Rev. B* **2005**, *72* (24), No. 241401.

(27) Blyholder, G. *J. Phys. Chem.* **1964**, *68* (10), 2772.

(28) Gajdos, M.; Eichler, A.; Hafner, J. *J. Phys.: Condens. Matter* **2004**, *16* (8), 1141–1164.

(29) Kamenetska, M.; Quek, S. Y.; Whalley, A. C.; Steigerwald, M. L.; Choi, H. J.; Louie, S. G.; Nuckolls, C.; Hybertsen, M. S.; Neaton, J. B.; Venkataraman, L. *J. Am. Chem. Soc.* **2010**, *132* (19), 6817–6821.